Phase diagram of a symmetric binary fluid in a porous matrix

Elisabeth Schöll-Paschinger,[1] Dominique Levesque,[2] Jean-Jacques Weis,[2] and Gerhard Kahl[1]
[1]*Institut für Theoretische Physik and Center for Computational Materials Science, TU Wien, Wiedner Hauptstraße 8-10, A-1040 Wien, Austria*
[2]*Laboratoire de Physique Théorique, UMR 8627, Bâtiment 210, Université de Paris–Sud, F-91405 Orsay Cedex, France*
(Received 12 May 2000; revised manuscript received 27 November 2000; published 13 June 2001)

The phase behavior of a binary symmetric fluid in thermal equilibrium with a porous matrix has been studied with the optimized random phase approximation and grand canonical Monte Carlo simulations. Depending on the matrix properties and the matrix-fluid and fluid-fluid interactions we find three types of phase diagram characterized by a tricritical point, a tricritical point with a triple point, or a critical end point. Small changes in the properties of the matrix or in the interactions are demonstrated to lead to drastic modifications of the phase diagram of the fluid, in qualitative agreement with observations in experimental studies. We show, in particular, that the change between the different types of phase diagram is triggered not only by the fluid-fluid interactions (internal parameters) but also by the properties of the matrix and of the matrix-fluid potentials (external parameters).

DOI: 10.1103/PhysRevE.64.011502 PACS number(s): 05.70.Fh, 64.70.Fx, 64.70.Ja

I. INTRODUCTION

In many technological applications where a liquid is in thermal equilibrium with a disordered porous matrix (such as catalysis, adsorption separation, enhanced oil recovery, or others) it is of great importance to understand the influence of the properties of the adsorbent matrix on the phase behavior of the fluid. The relevance of this problem is reflected in the large increase in the number of theoretical and experimental studies devoted to it (see, e.g., [1], and references therein).

Experimental studies of binary mixtures in both high (silica gels) [2] and low porosity (Vycor) [3] matrices are numerous and have shown persuasively that the phase behavior is markedly different from that of the bulk system under the same conditions. However, in these rather complex systems the combined influence of pore structure, randomness, wetting phenomena, capillary condensation, etc., on phase separation is not yet satisfactorily explained. Disentanglement of the roles of these various factors can, however, be done by studying well defined model systems, amenable to either theoretical analysis or computer simulations, in which these factors can be varied in a controlled way.

Such a theoretical approach is followed in the present paper for a model of a symmetric binary mixture adsorbed in a porous matrix formed by immobile particles modeled as hard spheres. It generalizes to the mixture case a method originally proposed by Madden and Glandt [4] and subsequently reformulated by Given and Stell [5–7]. In this method the system composed of the fluid and the porous matrix is described as an ensemble of equilibrium states of the fluid adsorbed in possible configurations of the matrix. The essence is to apply the replica trick to evaluate the two thermodynamic averages required to determine the properties of the adsorbed mixture—the first over the fluid particle configurations at given matrix arrangements, and the second over different matrix configurations. The replica trick [8] exploits a mathematical isomorphism between this partly quenched system and the limiting case of a corresponding equilibrium system that consists of the now mobile matrix particles and of s noninteracting identical copies of the fluid particles. This latter system can be treated by standard liquid state theories [9]. The properties of the quenched system are then obtained by considering the limit $s \to 0$ of the properties of the equilibrium system. Using this formalism one can derive the so-called replica Ornstein-Zernike equations (ROZ), analogous to the familiar Ornstein-Zernike equations in standard liquid state theory, which relate the different correlation functions of the system. From the knowledge of these the thermodynamic properties can be calculated [10–12].

As expected, the symmetric binary mixture case exhibits, even for the *pure* mixture, a much richer variety of phase diagrams than the one component system. Depending on the values of the coupling strengths of the fluid-fluid and matrix-fluid interactions, the three different phases equimolar gas (G), equimolar liquid (L), or nonequimolar (demixed) fluid (DF) that can be encountered are arranged in three types of phase diagram which, as in the pure mixture case, differ in the way the second order transition associated with demixing merges into a first order transition. In the case where the first order transition between the equimolar gas and equimolar liquid is absent, the λ line (critical line of the fluid demixing) ends at a tricritical point (type III) and a first order transition between an equimolar gas and a demixed fluid appears. In the case where the G-L transition exists, the λ line either ends at a tricritical point where a first order transition between an equimolar liquid and a demixed liquid appears (type II) or ends at a critical end point (CEP) on the G-L coexistence line (type I). In a mean-field study of a pure (bulk) symmetric binary mixture it was shown [13] that the transition between the different types of phase diagram is triggered by a parameter α, i.e., the ratio of the unlike to like interactions. Here we demonstrate that similar changes can also be induced by the parameters governing the matrix-matrix and matrix-fluid interactions. This scenario is confirmed by performing grand canonical Monte Carlo (GCMC) simulations [14].

Although our simple model (hard-sphere Yukawa interac-

tions are used throughout) does not allow a full description of the experimental systems it nevertheless can mimic their characteristic features and bring systematic parameter variations within practical reach.

The remaining part of the paper is organized as follows. After description of the potentials that characterize our model in Sec. II, we present briefly, in Sec. III, the optimized random phase approximation (ORPA) that is used as a closure to the ROZ equations and collect the expressions (free energy, chemical potential, and pressure) that are necessary to calculate phase diagrams. Section IV contains details of the GCMC simulations, in particular the distribution of numbers of particles and histogram reweighting methods that served to locate the various phase transitions. The section following (Sec. V) describes the results: comparison is made between simulation results and ORPA predictions and trends in the variation of the phase diagrams induced by the different system parameters are discussed. The paper is concluded with a summary of our main results.

II. THE SYSTEM

The system we have studied is a symmetric binary hard-sphere Yukawa mixture in equilibrium with a porous (hard-sphere) matrix. All the interactions of the system can be written as $[\beta=1/(k_BT)]$

$$\beta\Phi_{ij}(r)=\begin{cases}\infty, & r<\sigma\\ -\dfrac{K_{ij}}{r}\exp[-z(r-\sigma)], & r\geqslant\sigma.\end{cases} \tag{1}$$

A value 0 of index i or j denotes the matrix particles, while 1 and 2 denote the two components of the fluid. The diameter σ is assumed to be equal for all interactions and z is the screening length. The contact values K_{ij} are parametrized as follows:

$$K_{00}=0,\quad K_{11}=K_{22}, \tag{2}$$

$$K_{12}=\alpha K_{11},\quad K_{01}=K_{02}=yK_{11}. \tag{3}$$

We define a reduced temperature via $T^\star=\sigma/K_{11}$ (in the following $T^\star$ is denoted by T). Further system variables are the partial densities ρ_i of species i, the concentration of species 1 of the fluid $x=\rho_1/(\rho_1+\rho_2)$, the fluid density $\rho_f=\rho_1+\rho_2$, and the matrix density ρ_0 (densities will be given in units of σ^3 throughout the paper). In all calculations presented here, unless otherwise stated, the potentials have been truncated at $r_c=2.5\sigma$, and $z\sigma$ was chosen to be 2.5; this is for both the simulations and the theoretical calculations.

III. THERMODYNAMIC PERTURBATION THEORY

A. Structure and thermodynamics

In this section we present the ROZ equations generalized to the binary mixture case. We also give a summary of the relevant thermodynamic expressions that are needed in order to locate the phase transitions: they were obtained within the framework of the ORPA closure relation to the ROZ equations. For full details of the derivation we refer the reader to Ref. [12].

The ROZ equations relate the fluid-fluid, matrix-fluid, and matrix-matrix direct $c_{ij}(r)$ and total $h_{ij}(r)$ correlation functions. They can be written in compact form as

$$h_{00}=c_{00}+\rho_0 c_{00}\otimes h_{00}, \tag{4}$$

$$\mathbf{h}_{01}=\mathbf{c}_{01}+\mathbf{h}_{01}\otimes\rho_0 c_{00}+\boldsymbol{\rho}_1\mathbf{h}_{11}\otimes\mathbf{c}_{01}-\boldsymbol{\rho}_1\mathbf{h}_{12}\otimes\mathbf{c}_{01},$$

$$\mathbf{h}_{11}=\mathbf{c}_{11}+\mathbf{h}_{01}\otimes\rho_0\mathbf{c}_{01}^{\mathrm{T}}+\boldsymbol{\rho}_1\mathbf{h}_{11}\otimes\mathbf{c}_{11}-\boldsymbol{\rho}_1\mathbf{h}_{12}\otimes\mathbf{c}_{12},$$

$$\mathbf{h}_{12}=\mathbf{c}_{12}+\mathbf{h}_{01}\otimes\rho_0\mathbf{c}_{01}^{\mathrm{T}}+\boldsymbol{\rho}_1\mathbf{h}_{12}\otimes\mathbf{c}_{11}+\boldsymbol{\rho}_1\mathbf{h}_{11}\otimes\mathbf{c}_{12}-2\boldsymbol{\rho}_1\mathbf{h}_{12}\otimes\mathbf{c}_{12},$$

where the superscript T denotes the transpose of a vector and $\otimes$ stands for a convolution. The following matrix notation has been introduced [12]:

$$\boldsymbol{\rho}_1=\begin{pmatrix}\rho_1 & 0\\ 0 & \rho_2\end{pmatrix},\quad \mathbf{h}_{01}=\begin{pmatrix}h_{01}\\ h_{02}\end{pmatrix},\quad \mathbf{c}_{01}=\begin{pmatrix}c_{01}\\ c_{02}\end{pmatrix}, \tag{5}$$

$$\mathbf{h}_{11}=\begin{pmatrix}h_{11} & h_{12}\\ h_{12} & h_{22}\end{pmatrix},\quad \mathbf{c}_{11}=\begin{pmatrix}c_{11} & c_{12}\\ c_{12} & c_{22}\end{pmatrix},$$

$$\mathbf{h}_{12}=\begin{pmatrix}h_{13} & h_{14}\\ h_{14} & h_{24}\end{pmatrix},\quad \mathbf{c}_{12}=\begin{pmatrix}c_{13} & c_{14}\\ c_{14} & c_{24}\end{pmatrix}, \tag{6}$$

where h_{13} (h_{24}) is the $(s\to 0)$ limit of the correlation function between particles of species 1 (2) of different replicas. Further, h_{14} is the $(s\to 0)$ limit of the correlation function between unlike particles of different replicas. Within the present framework, which describes fluids in contact with porous media, these functions are called the ''blocking parts'' of the correlation functions. The ROZ equations form a set of nine integral equations, eight of them being coupled.

To close these equations we have chosen the ORPA [15]. The basic assumption in this framework is that all pair potentials can be split into a reference part (index ''r'') and a perturbation part (index ''p''), i.e.,

$$\Phi_{ij}(r)=\Phi_{\mathrm{r};ij}(r)+\Phi_{\mathrm{p};ij}(r). \tag{7}$$

In the present study the $\Phi_{\mathrm{r};ij}(r)$'s are hard-sphere potentials characterized by one single hard-sphere diameter σ. Equation (7) defines $\Phi_{\mathrm{p};ij}(r)$ up to a finite contribution inside the core region. In a similar way, the correlation functions are split into reference and perturbation parts. For convenience we define the matrices $(C)=\sqrt{\rho_i\rho_j}\,c_{ij}$ and $(C_r)_{ij}=\sqrt{\rho_i\rho_j}\,c_{r;ij}$. The ORPA closure relation assumes that

$$c_{\mathrm{p};ij}(r)=-\beta\Phi_{\mathrm{p};ij}(r),\quad r\geqslant\sigma, \tag{8}$$

while inside the core region $(r<\sigma)$ the $c_{\mathrm{p};ij}$'s are chosen to guarantee

$$h_{\mathrm{p};ij}(r)=0\quad\text{for}\quad r<\sigma. \tag{9}$$

Applying the ORPA to the replicated system and taking the limiting case $s \to 0$ one obtains the properties of the partly quenched system.

The free energy density of this system, $\overline{A^\star}(=-\beta\overline{A}/V)$, is obtained from the free energy of the replicated system, $[A^{\rm rep}(s)]^\star$, via $\overline{A^\star}=\lim_{s\to 0}(d/ds)[A^{\rm rep}(s)]^\star$ [10,16]. In the following calculations only the difference between $\overline{A^\star}$ and the free energy of the reference system, $\overline{A_{\rm r}^\star}$, is required,

$$\begin{aligned}\overline{A^\star}-\overline{A_{\rm r}^\star}=&-\mathcal{A}[\mathsf{C}]+\mathcal{A}[\mathsf{C}_{\rm r}]+\frac{1}{2}[\rho_1^2\tilde{c}_{{\rm p};11}+\rho_2^2\tilde{c}_{{\rm p};22}\\&+2\rho_0\rho_1\tilde{c}_{{\rm p};01}+2\rho_0\rho_2\tilde{c}_{{\rm p};02}+2\rho_1\rho_2\tilde{c}_{{\rm p};12}]_{q=0}\\&-\frac{1}{2}[\rho_1 c_{{\rm p};11}+\rho_2 c_{{\rm p};22}]_{r=0},\end{aligned}\tag{10}$$

where the functional $\mathcal{A}[\mathsf{C}]$ is defined as

$$\begin{aligned}\mathcal{A}[\mathsf{C}]=&\frac{1}{2(2\pi)^3}\int d\mathbf{q}\Bigg\{\ln\{(1-\rho_1\tilde{c}_{11}^c)(1-\rho_2\tilde{c}_{22}^c)\\&-\rho_1\rho_2[\tilde{c}_{12}^c]^2\}\\&-\frac{1}{[1-\rho_1\tilde{c}_{11}^c][1-\rho_2\tilde{c}_{22}^c]-\rho_1\rho_2[\tilde{c}_{12}^c]^2}\\&\times\Bigg[\rho_1\tilde{c}_{13}(1-\rho_2\tilde{c}_{22}^c)+\rho_2\tilde{c}_{24}(1-\rho_1\tilde{c}_{11}^c)\\&+2\rho_1\rho_2\tilde{c}_{14}\tilde{c}_{12}^c+\frac{\rho_0}{1-\rho_0\tilde{c}_{00}}[\rho_1\tilde{c}_{01}^2(1-\rho_2\tilde{c}_{22}^c)\\&+\rho_2\tilde{c}_{02}^2(1-\rho_1\tilde{c}_{11}^c)+2\rho_1\rho_2\tilde{c}_{01}\tilde{c}_{02}\tilde{c}_{12}^c]\Bigg]\Bigg\}\end{aligned}\tag{11}$$

and $\mathcal{A}[\mathsf{C}_{\rm r}]$ is obtained from the above expression by substituting the c_{ij}'s by $c_{{\rm r};ij}$'s. In the above expressions a tilde denotes the Fourier transform of a function. Further, we have introduced the ''connected'' parts of the correlation functions, defined as

$$c_{11}^c=c_{11}-c_{13},\quad c_{12}^c=c_{12}-c_{14},\quad c_{22}^c=c_{22}-c_{24}.\tag{12}$$

Using the expression (10) for the free energy one can show that

$$\left(\frac{\delta\overline{A^\star}}{\delta c_{{\rm p};ij}}\right)(r)=\frac{2-\delta_{ij}}{2}\rho_i\rho_j[g_{{\rm r};ij}(r)+h_{{\rm p};ij}(r)],\tag{13}$$

which means that the minimization of $\overline{A^\star}$ with respect to variations of the $c_{{\rm p};ij}(r)$ inside the core region is equivalent to the hard-core condition (9).

The chemical potentials $\mu_i=\mu_i^{\rm id}+\mu_{{\rm r};i}^{\rm ex}+\mu_{{\rm p};i}$ are calculated as follows (''ex'' denotes the excess part over the ideal part ''id''): the reference parts are obtained via numerical integration of the compressibility equation, i.e.,

$$\left(\frac{\partial\beta\mu_{{\rm r};1}^{\rm ex}}{\partial\rho_f}\right)_{T,x,\rho_0}=-x[\tilde{c}_{{\rm r};11}^c]_{q=0}-(1-x)[\tilde{c}_{{\rm r};12}^c]_{q=0},\tag{14}$$

$$\left(\frac{\partial\beta\mu_{{\rm r};2}^{\rm ex}}{\partial\rho_f}\right)_{T,x,\rho_0}=-(1-x)[\tilde{c}_{{\rm r};22}^c]_{q=0}-x[\tilde{c}_{{\rm r};12}^c]_{q=0},\tag{15}$$

using as an integration constant at $\rho_f=0$ the Carnahan-Starling expression for the excess chemical potential of a one-component sytem of hard spheres at packing fraction $\eta=(\pi/6)\rho_0\sigma^3$ [17],

$$\beta\mu_{{\rm r};i}^{\rm ex}(\rho_f=0)=\frac{8\eta-9\eta^2+3\eta^3}{(1-\eta)^3},\quad i=1,2.\tag{16}$$

Further, the ideal parts of the chemical potentials are given by $\beta\mu_i^{\rm id}=\ln\rho_i (i=1,2)$ and the perturbation parts of the μ_i's by

$$\begin{aligned}\beta\mu_{{\rm p};1}=&\beta\mu_1-\beta\mu_{{\rm r};1}\\=&-[\rho_f x\tilde{c}_{{\rm p};11}+\rho_0\tilde{c}_{{\rm p};01}+\rho_f(1-x)\tilde{c}_{{\rm p};12}]_{q=0}\\&+\frac{1}{2}[c_{{\rm p};11}]_{r=0},\end{aligned}\tag{17}$$

$$\begin{aligned}\beta\mu_{{\rm p};2}=&\beta\mu_2-\beta\mu_{{\rm r};2}\\=&-[\rho_f(1-x)\tilde{c}_{{\rm p};22}+\rho_0\tilde{c}_{{\rm p};02}+\rho_f x\tilde{c}_{{\rm p};12}]_{q=0}\\&+\frac{1}{2}[c_{{\rm p};22}]_{r=0}.\end{aligned}\tag{18}$$

The pressure $P=P^{\rm id}+P_{\rm r}^{\rm ex}+P_{\rm p}$ is calculated as follows: the ideal contribution is $\beta P^{\rm id}=\rho_f$; the reference part to the pressure is obtained via numerical integration of

$$\begin{aligned}\left(\frac{\partial\beta P_{\rm r}^{\rm ex}}{\partial\rho_f}\right)_{T,x,\rho_0}=&-\rho_f\{x^2[\tilde{c}_{{\rm r};11}^c]_{q=0}+2x(1-x)[\tilde{c}_{{\rm r};12}^c]_{q=0}\\&+(1-x)^2[\tilde{c}_{{\rm r};22}^c]_{q=0}\}.\end{aligned}\tag{19}$$

The integration constants are irrelevant if one wants to determine only the phase diagram.

Finally, the perturbation part of the pressure is calculated from the Gibbs-Duhem relation

$$\beta P_{\rm p}=\overline{A^\star}-\overline{A_{\rm r}^\star}+\beta\sum_{i=1,2}\rho_i\mu_{{\rm p};i},\tag{20}$$

where the difference of the free energies is taken from Eq. (10).

B. Calculation of the phase diagram

We have determined the phase diagrams by equating, at a given temperature T, the pressure P and the chemical potentials μ_i of the coexisting phases. The general equilibrium conditions read

$$\mu_i(\rho_f,x,T)=\mu_i(\rho_f',x',T), \quad i=1,2, \tag{21}$$

$$P(\rho_f,x,T)=P(\rho_f',x',T), \tag{22}$$

where the thermodynamic states of the coexisting phases are given by (ρ_f,x) and (ρ_f',x'). The symmetry of the system, expressed via $\Phi_{01}=\Phi_{02}$ and $\Phi_{11}=\Phi_{22}$, leads to

$$\mu_1(\rho_f,x,T)=\mu_2(\rho_f,1-x,T), \tag{23}$$

$$P(\rho_f,x,T)=P(\rho_f,1-x,T). \tag{24}$$

Using these relations we now proceed to the calculation of the phase diagrams. The G-L coexistence is obtained by solving the set of equations

$$\mu_i(\rho_f,x=1/2,T)\equiv\mu_f(\rho_f,x=1/2,T)=\mu_f(\rho_f',x=1/2,T), \tag{25}$$

$$P(\rho_f,x=1/2,T)=P(\rho_f',x=1/2,T). \tag{26}$$

For the G-DF and L-DF transitions we proceed in two steps. First we determine the phase diagram of the demixing transition, i.e., we search for two coexisting states with the same fluid density but different compositions by setting $\rho_f'=\rho_f$ and determining the concentrations x and x' of the coexisting phases. Due to the symmetry of the interactions $x'=1-x$ must hold. Then Eq. (22) is automatically satisfied, while Eq. (21) reduces to

$$\mu_1(\rho_f,x,T)=\mu_2(\rho_f,x,T), \tag{27}$$

which defines the line $x(\rho_f)$ of the second order demixing transition if it exists. Along this line the chemical potentials of the two species are equal by construction and denoted by $\mu_f(\rho_f,x(\rho_f),T)$. In a second step the solution of the two equations

$$\mu_f(\rho_f,x=1/2,T)=\mu_f(\rho_f',x(\rho_f'),T), \tag{28}$$

$$P(\rho_f,x=1/2,T)=P(\rho_f',x(\rho_f'),T) \tag{29}$$

gives the density of the equimolar gas or fluid, ρ_f, and that of the demixed fluid, ρ_f', with concentrations $x(\rho_f')$ and $1-x(\rho_f')$, in equilibrium.

As we approach the critical or tricritical point the above systems of equations become ill conditioned. In all the phase diagrams presented in Sec. V we have plotted the coexistence curves as far as reliable numerical solutions were available, the open segments representing those regions where no numerical solution could be found.

For the determination of the critical temperature and density, T_c and ρ_c, the results were extrapolated under the assumption that the coexistence curve can be described by a scaling type law and the law of rectilinear diameters, i.e.,

$$\rho_l-\rho_g=B(T-T_c)^{\beta}, \quad (\rho_l+\rho_g)/2=\rho_c+A(T-T_c). \tag{30}$$

Equations (30) were fitted to the coexistence curves by taking A,B, and β as adjustable parameters. Due to the well-known fact that the ORPA (being a conventional liquid state theory) fails to describe correctly the critical region [18], the values of β (generally between 1/3 and 1/2 depending on matrix density) obtained by the curve fitting should not be considered as reliable estimates of a critical exponent.

C. Numerical details

For the numerical solution of the ORPA we have discretized the correlation functions in both r and q space, using typically 1024 grid points and a mesh size of $\Delta r=0.01\sigma$. For a given system, we first calculate the correlation functions $h_{\mathrm{r};ij}$ and $c_{\mathrm{r};ij}$ of the reference system by solving the ROZ equations (4) along with the Percus-Yevick (PY) closure [9] using the Labik-Malijevsky-Vonka algorithm [19] adapted to the present problem [20]. Then we solve the ORPA by minimizing $\mathcal{A}$ [Eq. (11)] to obtain the correlation functions $h_{\mathrm{p};ij}$ and $c_{\mathrm{p};ij}$. The advantage of this minimization algorithm lies in the fact that an explicit calculation of the functional is not required; we only need its derivatives, i.e., the $h_{\mathrm{p};ij}$'s, which we easily obtain from the so-called residual ROZ equations [21]. Starting from an initial guess for the direct correlation functions inside the core region (for instance, the simple RPA expression or the solution at some lower density) we calculate improved correlation functions with a steepest descent method until we obtain a minimum in the functional within a sufficient accuracy. The step size in this search is triggered by a parameter that expresses quantitatively the degree of violation of the core condition Eq. (9) by the resulting perturbation parts of the total correlation functions $h_{\mathrm{p};ij}$ (cf. [12]). The iterative algorithm was considered to be converged if the difference $\Delta\Gamma_{ij}$ between two successive values of the functions $\Gamma_{ij}=(h_{ij}-c_{ij})r$ satisfied

$$\sum_{ij}\sum_{l}[\Delta\Gamma_{ij}(r_l)]^2\Delta r<10^{-5}. \tag{31}$$

In Eq. (31) the first summation is done over all pairs of indices while the second sum is taken over all grid points of the r mesh. For each system the ROZ equations have been solved along isotherms separated by $\Delta T=0.002$ (0.0001 near critical regions) with a grid size of 0.005 in density and 0.0125 in concentration.

Phase diagrams were determined from numerical solution of the equilibrium conditions Eqs. (25)–(29); these coupled nonlinear equations were solved via a generalized Newton-Raphson procedure.

IV. COMPUTER SIMULATIONS

The gas-liquid and demixing transitions of the symmetric binary mixture specified in the preceding section have been

studied with a grand canonical simulation technique. The fluid mixture is adsorbed in a porous matrix formed by immobile particles modeled as hard spheres. As already outlined in Sec. III, two thermodynamic averages are required to determine the properties of the adsorbed mixture: one corresponds to the determination of the equilibrium properties of the mixture in a given matrix configuration, the other to the mean values of these properties in a properly weighted ensemble of matrix configurations. In our simulation the weighting procedure for the matrix configurations uses the canonical ensemble for a hard-sphere system at a given density ρ_0. The equilibrium properties of the two adsorbed fluids are calculated according to the standard scheme of the GCMC simulation at a chemical potential $\mu_f=\mu_1=\mu_2$ equal for the two fluids.

Typically a simulation run starts by selecting randomly a configuration of the matrix from those generated in a canonical ensemble simulation of a hard-sphere system at density ρ_0 in a cube of volume $500\sigma^3$ with periodic boundary conditions. The equilibrium state of the mixture at chemical potential μ_f and temperature T is then determined by performing three types of trial move: a random insertion of a new particle into the volume V containing the fixed matrix particles, a random deletion, and a random displacement of a particle. These three trial moves are accepted following a Metropolis algorithm corresponding to weighting the fluid particle configurations in a grand canonical ensemble.

The matrix densities considered are $\rho_0 = 0$, 0.05, 0.15, and 0.30, and the parameters y and α that characterize the matrix-fluid and fluid-fluid interactions (see Sec. II) are chosen to be 1 and 0.7, respectively. In the case $\rho_0=0$ the properties of the mixture are evaluated without the matrix. The influence of the latter on the location of the phase transition can be estimated with respect to this reference phase diagram.

The gas-liquid equilibria and the demixing transitions have been calculated for the case of a *pure* mixture by calculating the histograms of the number of particles of the two species, N_1 and N_2. For a given configuration of the N_1 and N_2 particles with positions $\mathbf{R}^1_{N_1}=\{\mathbf{r}^1_1,\ldots,\mathbf{r}^1_{N_1}\}$ and $\mathbf{R}^2_{N_2}=\{\mathbf{r}^2_1,\ldots,\mathbf{r}^2_{N_2}\}$, we have the histogram

$$P(N_1,N_2,U_f,\mu_f,T,V) = \frac{1}{N_1!\,N_2!}\,\frac{e^{\beta\mu_f(N_1+N_2)}e^{-\beta U_f(\mathbf{R}^1_{N_1},\mathbf{R}^2_{N_2})}}{\Xi(\mu_f,V,T)}, \quad (32)$$

where $U_f(\mathbf{R}^1_{N_1},\mathbf{R}^2_{N_2})$ is the interaction energy of the particles of the mixture and $\Xi(\mu_f,V,T)$ the grand partition function.

By summing over the values of $U_f(\mathbf{R}^1_{N_1},\mathbf{R}^2_{N_2})$, keeping N_1 and N_2 fixed, i.e., by integrating over the particle positions $\mathbf{R}^1_{N_1}$ and $\mathbf{R}^2_{N_2}$, we obtain

$$P_f(N_1,N_2,\mu_f,T,V) = \frac{1}{N_1!\,N_2!}\,\frac{e^{\beta\mu_f(N_1+N_2)}\int_V e^{-\beta U_f(\mathbf{R}^1_{N_1},\mathbf{R}^2_{N_2})}d\mathbf{R}^1_{N_1}\,d\mathbf{R}^2_{N_2}}{\Xi(\mu_f,V,T)}. \quad (33)$$

It will be useful to define histograms for the sum and difference of species numbers,

$$P_m(N_f,\mu_f,T,V) = \sum_{N_1,N_2}\delta(N_f-(N_1+N_2))P_f(N_1,N_2,\mu_f,T,V) \quad (34)$$

and

$$P_d(N_d,\mu_f,T,V) = \sum_{N_1,N_2}\delta(N_d-(N_1-N_2))P_f(N_1,N_2,\mu_f,T,V). \quad (35)$$

For the systems studied here, the histogram P_f is symmetric in N_1 and N_2. In a three dimensional representation, for an equimolar mixture (where on average N_1 is equal to N_2), P_f presents a peak in the (N_1,N_2) plane on the line $N_1=N_2$ at coordinates $N_1=N_2\simeq\overline{N}_f/2$ ($\overline{N}_f$ is the mean value of N_f) corresponding to a density of the mixture $\rho_f=\overline{N}_f/V$. The different phase transitions are characterized by the existence of several peaks in P_f.

The gas-liquid transition between the equimolar fluids corresponds to the existence of two peaks, located along the line $N_1=N_2$ at coordinates $N_1=N_2\simeq\overline{N}^g_f/2$ and $N_1=N_2\simeq\overline{N}^l_f/2$, associated with the gas and liquid densities $\rho^g_f\simeq\overline{N}^g_f/V$ and $\rho^l_f\simeq\overline{N}^l_f/V$, respectively. The coexistence between an equimolar gas or liquid and a demixed fluid mixture results in the appearance of three peaks. One is situated on the line $N_1=N_2$ at $N_1=N_2\simeq\overline{N}^g_f/2$ or $N_1=N_2\simeq\overline{N}^l_f/2$, corresponding to the density of the equimolar gas or liquid phase. The two other peaks are symmetric with respect to the line $N_1=N_2$ and are located in the (N_1,N_2) plane on the line $N_1=-N_2+\overline{N}^{df}_f$ where $\overline{N}^{df}_f$ corresponds to the density of the demixed fluid, $\rho^{df}_f=\overline{N}^{df}_f/V$. The existence of a second order demixing transition becomes apparent by a progressive broadening of the peak of the equimolar phase situated on the line $N_1=N_2$. As μ_f is increased at fixed T, it splits into two peaks symmetrical with respect to the line $N_1=N_2$ and located on the line $N_1=-N_2+\overline{N}^{df}_f$.

Since the gas-liquid transition is of first order, the value of μ_f, for which the gas and liquid phases (equimolar or demixed) are in equilibrium along an isotherm, is estimated by the value where the two or three peaks of the histogram P_f are of equal height, i.e., where the maximum probabilities of the different phases are equal.

The histogram P_m can be used to identify the first order fluid-fluid transitions: it then shows two peaks at different values of N_f. If it is a gas-liquid transition without demixing, the two values for N_f at which these peaks occur correspond to nearly identical values of N_1 and N_2, or, equivalently, to a single peak in the histogram P_d for $N_d=0$. If the first order fluid-fluid transition is a demixing transition, then the histogram P_d has three peaks: one of these peaks at N_d

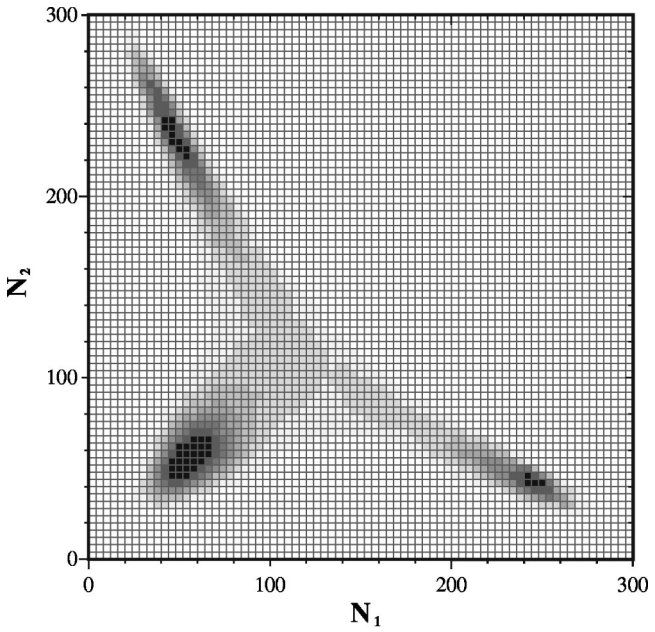

FIG. 1. Histogram $\overline{P_f}$ (as defined in the text) for the equimolar-gas–demixed-liquid transition of a binary fluid in contact with a porous matrix ($\rho_0=0.15$) as a function of N_1 and N_2 at $T=0.61$. Increasing gray levels indicate increasing values of the histogram.

$=0$ corresponds to the gas phase at low density and equal concentration, and the other two represent the demixed phase. The finite values of N_d (equal in absolute value but with opposite sign) at which the peaks occur quantify the difference in the concentrations of the two fluids in the mixture: this corresponds, taking into account the symmetry of the system, with equal probability to either the case $N_1 > N_2$ or the case $N_1 < N_2$.

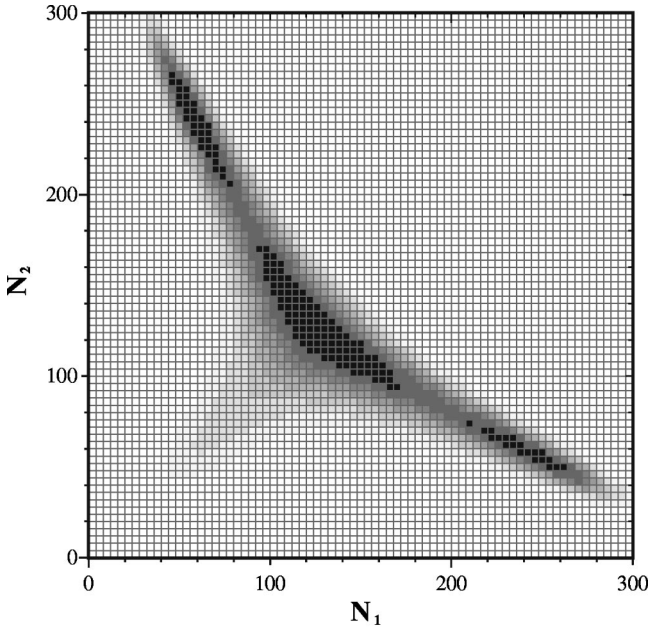

FIG. 2. Histogram $\overline{P_f}$ (as defined in the text) for equimolar-liquid–demixed-fluid equilibrium of a binary fluid in contact with a porous matrix ($\rho_0=0.05$) as a function of N_1 and N_2 at $T=0.68$. Increasing gray levels indicate increasing values of the histogram.

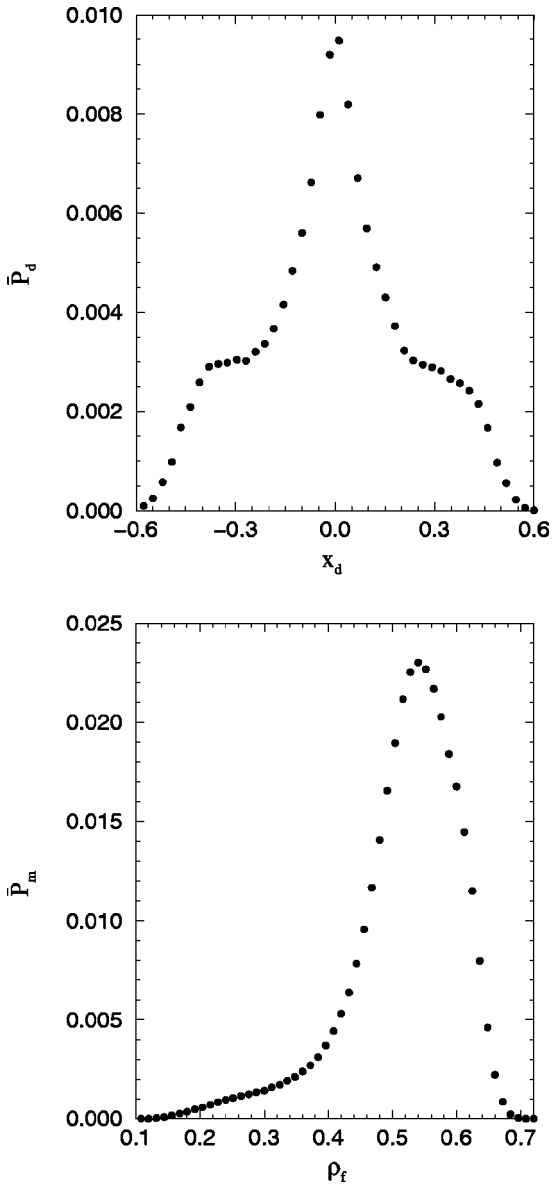

FIG. 3. Histograms $\overline{P_d}$ ($\overline{P_m}$) (as defined in the text) for equimolar-liquid–demixed-fluid equilibrium of a binary fluid in contact with a porous matrix ($\rho_0=0.05$) as a function of $x_d = N_d/N(\rho_f)$ at $T=0.68$.

As already mentioned above, the second order demixing transition is accompanied by a broadening of the peak in P_f along the line $N_1=-N_2+\overline{N}_f^{df}$, and, as a consequence, of the peak in P_d at $N_d=0$, followed by a splitting into two symmetric peaks as μ_f increases. The location of the transition line is obtained by searching for the maximum value of the width of the peak at $N_d=0$ before it splits into two separate peaks; this is approximately equivalent to looking for the largest value of $\langle N_d^2 \rangle$ while the histogram P_d still has only one peak at $N_d=0$.

In the presence of a matrix, for a configuration $\mathbf{R}^0_{N_0} = \{\mathbf{r}_1^0, \ldots, \mathbf{r}_{N_0}^0\}$ defined by the (fixed) positions of the matrix

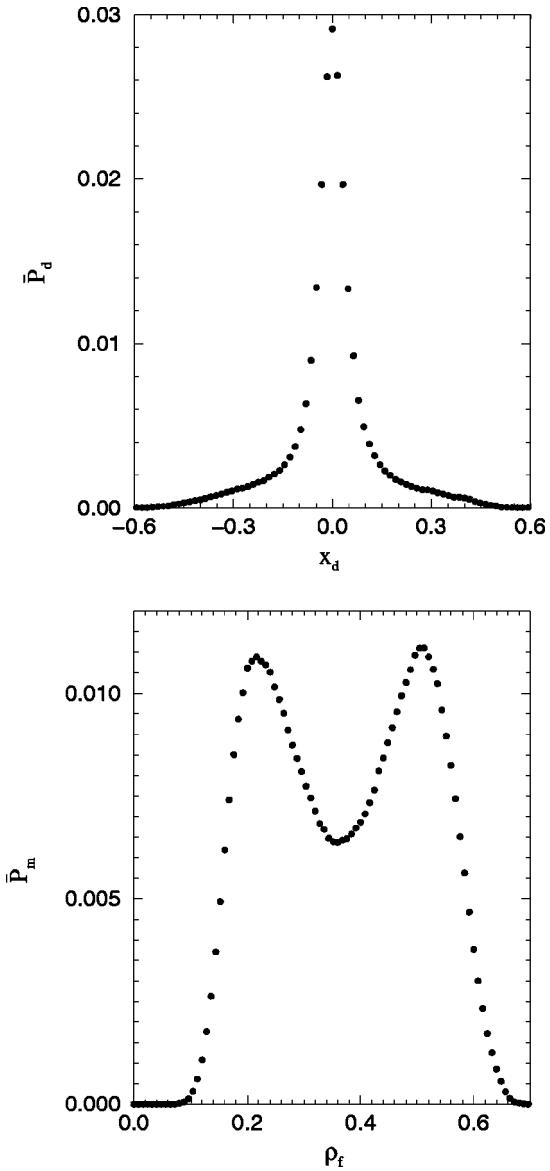

FIG. 4. Same as Fig. 3 but for an equimolar-gas–equimolar-liquid equilibrium.

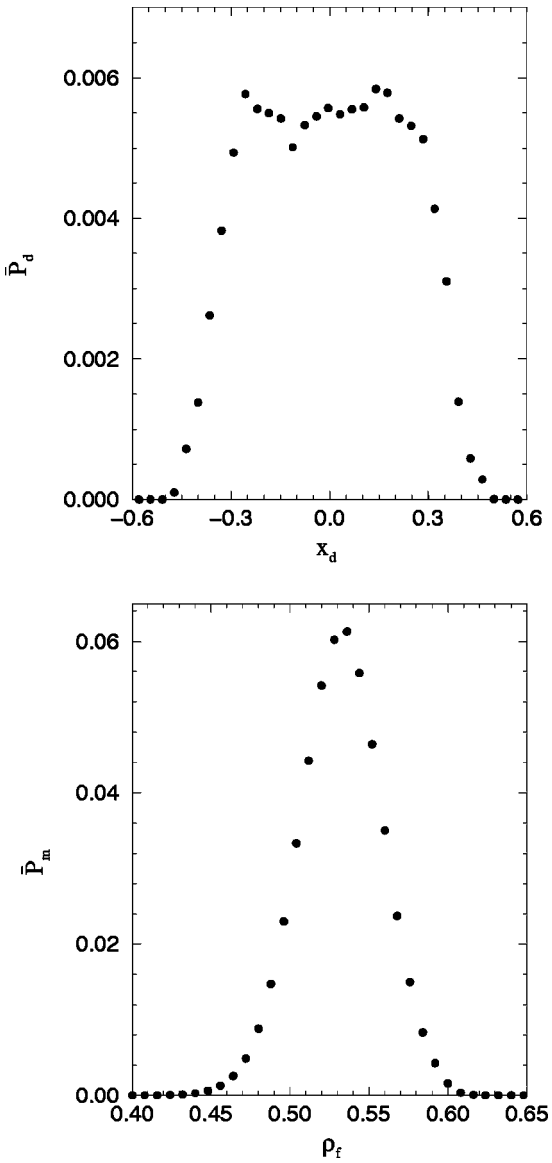

FIG. 5. Histograms $\overline{P_d}$ ($\overline{P_m}$) (as defined in the text) for the second order demixing transition of a binary fluid in contact with a porous matrix ($\rho_0=0.15$) as a function of $x_d=N_d/N(\rho_f)$ at $T=0.65$.

particles, the energy of the mixture will be a function of $\mathbf{R}^0_{N_0}$, implying a similar dependence for the histogram

$$P_f(N_1,N_2,\mu_f,T,V;\mathbf{R}^0_{N_0}) = \frac{1}{N_1!\,N_2!} \times \frac{e^{\beta\,\mu_f(N_1+N_2)}\int_V e^{-\beta U_f(\mathbf{R}^1_{N_1},\mathbf{R}^2_{N_2},\mathbf{R}^0_{N_0})} d\mathbf{R}^1_{N_1}\,d\mathbf{R}^2_{N_2}}{\Xi(\mu_f,V,T;\mathbf{R}^0_{N_0})}, \tag{36}$$

as well as for the histograms P_m and P_d derived from P_f.

The calculation of the histograms in the presence of a matrix therefore requires a canonical average over the configurations $\mathbf{R}^0_{N_0}$, according to

$$\overline{P_f}(N_1,N_2,\mu_f,T,V) = \frac{1}{Z_0}\int_V e^{-\beta U(\mathbf{R}^0_{N_0})} \times P_f(N_1,N_2,\mu_f,T,V;\mathbf{R}^0_{N_0})\,d\mathbf{R}^0_{N_0} \tag{37}$$

(and similar expressions for the histograms $\overline{P_m}$ and $\overline{P_d}$). The locations of the phase transitions from these histograms are made in a similar way as described above for the case of the mixture in the absence of the matrix. They hence rely on the values of N_1 and N_2 having maximum probabilities that in

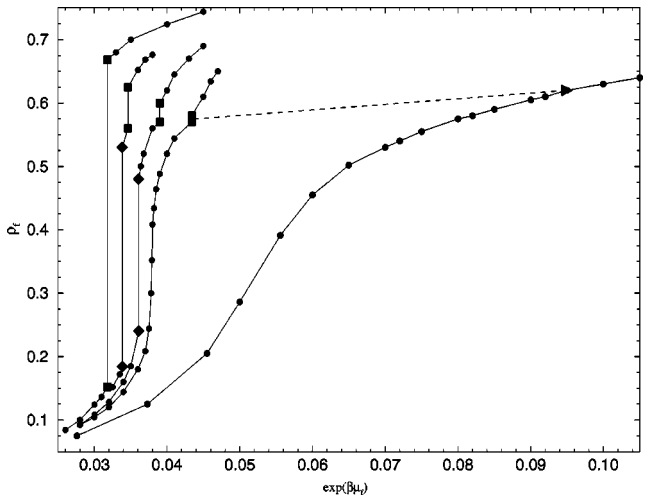

FIG. 6. Monte Carlo isotherms ρ_f versus fugacity $\exp(\beta\mu_f)$, at $T=0.70$, 0.71, 0.72, 0.73, and 0.80 (from left to right) for a bulk binary mixture. Solid triangles, second order demixing; solid squares, *G-DF* or *L-DF* equilibrium; black diamonds, *G-L* equilibrium. The dashed line is a linear interpolation between second order demixing points on isotherms, giving an approximate location of the λ line.

the case of a first order transition are equal (equal heights of the peaks in the histogram $\overline{P_f}$).

Once a certain number of simulations has been performed one can apply the histogram reweighting method [22] to determine the values of μ_f that lead to peaks of equal heights in $\overline{P_f}$. This method has been used in the literature to study the phase transitions of binary mixtures (see [23]) and can be applied here straightforwardly to the case of a pure mixture ($\rho_0=0$). The histogram P at chemical potential μ_f can be computed from n calculated histograms with chemical potentials $\mu_f^1, \ldots, \mu_f^n$ according to the expression

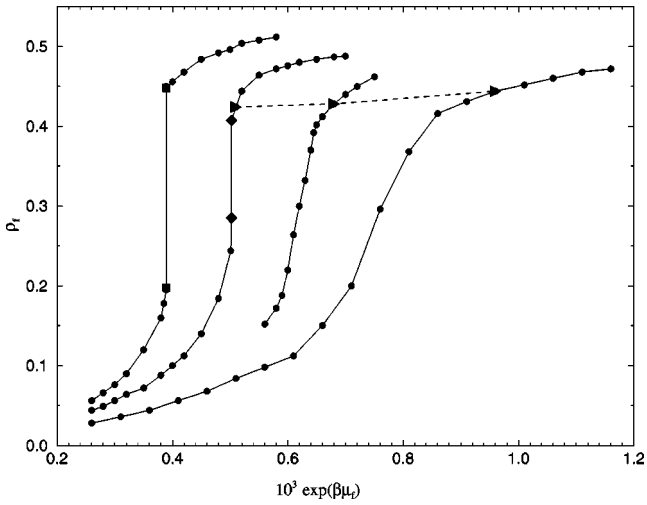

FIG. 7. Adsorption isotherms ρ_f versus fugacity $\exp(\beta\mu_f)$, at $T=0.49$, 0.50, 0.51, and 0.52 (from left to right) for a binary mixture in contact with a porous matrix of density $\rho_0=0.30$. Symbols as in Fig. 6.

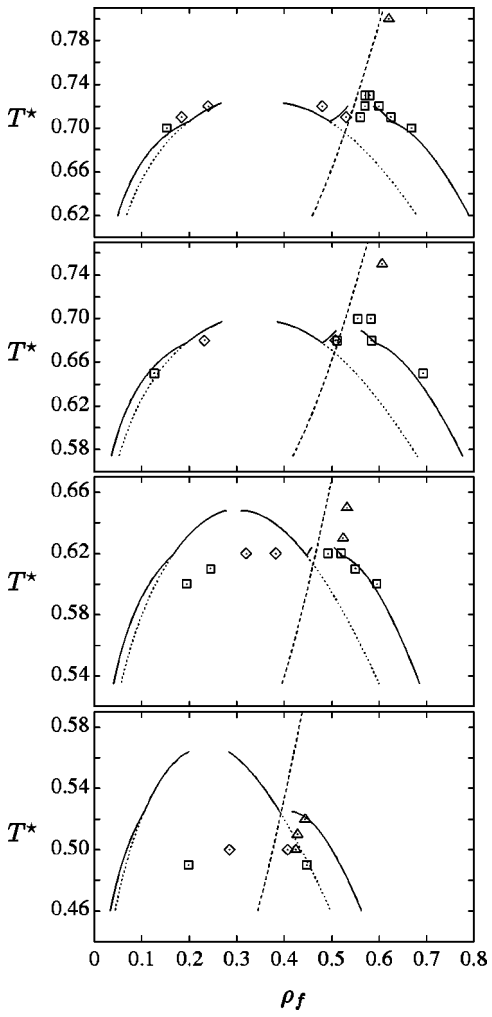

FIG. 8. Variation with matrix density ρ_0 of the phase diagram of a binary fluid mixture in contact with a porous matrix ($\alpha=0.7$, $y=1$, and $z\sigma=2.5$): comparison between MC and ORPA results. $\rho_0=0$,0.05, 0.15, and 0.30 (from top to bottom). Symbols: GCMC simulations (diamonds, *G-L* equilibrium; squares, *G-DF* or *L-DF* equilibrium; triangles, λ line). Lines: ORPA results (full line, *G-L*,*G-DF*, or *L-DF* coexistence curve; dotted line, metastable *G-L* transitions; dashed line, λ line).

$$P(N_1,N_2,U_f,\mu_f,T,V) = \frac{\sum_{i=1,n} P(N_1,N_2,U_f,\mu_f^i,T,V)e^{\beta\mu_f(N_1+N_2)}e^{-\beta U_f}}{\sum_{i=1,n} s_i e^{\beta\mu_f^i(N_1+N_2)}e^{-\beta U_f}e^{-f_i}}, \tag{38}$$

where $\exp(-f_i)=\Xi(\mu_f)/\Xi(\mu_f^i)$ and s_i is the number of entries in histogram P at chemical potential μ_f^i. The values of f_i are evaluated self-consistently.

In the presence of the matrix the histograms depend on the configuration of the matrix. Equation (38) allows us to calculate the histogram $P(N_1,N_2,U_f,\mu_f,T,V;\mathbf{R}_{N_0}^0)$ from the histograms calculated with different chemical potentials

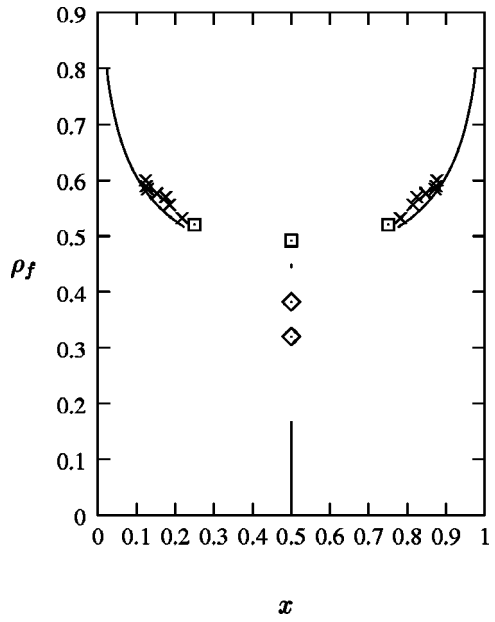

FIG. 9. Demixing transition of a binary fluid in contact with a porous matrix of density $\rho_0=0.15$ ($\alpha=0.7$, $y=1$, and $z\sigma=2.5$): ρ_f as a function of concentration x for $T=0.62$. The symbols denote GCMC simulations (diamonds, *G-L* equilibrium; squares, *L-DF* equilibrium; crosses, first order demixing transition), the lines the ORPA results.

for the same configuration $\mathbf{R}^0_{N_0}$. The average over the histograms $P(N_1,N_2,U_f,\mu_f,T,V;\mathbf{R}^0_{N_0})$ that are calculated in this way is then obtained via Eq. (37). This reweighting procedure can be advantageously replaced by an approximated procedure, where Eq. (38) is applied to the histograms averaged over the configurations of the matrix, substituting in $\exp(-f_i)$ an average function $\overline{\Xi}(\mu)$ independent of the $\mathbf{R}^0_{N_0}$ for the partition functions $\Xi(\mu;\mathbf{R}^0_{N_0})$. In this work the validity of this approximate procedure to determine the chemical potential that corresponds to a phase transition has been checked by performing simulations at the transition chemical potentials determined in this way.

Figures 1 and 2 give examples of the histograms $\overline{P_f}$ projected onto the (N_1,N_2) plane for the first order *G-DF* and *L-DF* transitions. Figure 2 demonstrates the difficulties encountered in an accurate location of the phase transitions by means of $\overline{P_m}$ and $\overline{P_d}$. These histograms, corresponding to projections of $\overline{P_f}$ onto planes located at the lines $N_1=N_2$ or $N_1=-N_2$, respectively, are given in Fig. 3 and clearly show that their peaks accumulate contributions stemming from the peaks of $\overline{P_f}$ which are associated with different phases. The possibility of such a superposition biasing the heights and widths of the peaks of $\overline{P_m}$ and $\overline{P_d}$ justified the use of $\overline{P_f}$ to locate the transitions. As illustrated in Figs. 4 and 5 such ambiguities do not occur for the *G-L* transition and the second order demixing transition. The *G-L* transition is well identified by the existence of two peaks of equal height in $\overline{P_m}$ and the symmetric peak in $\overline{P_d}$ at $x_d=N_d/N=0$. The onset of the second order transition is clearly visible from the very broad peak in $\overline{P_d}$, which signals the expected large fluctuations of the relative concentration of the two species on the λ line, while the peak in $\overline{P_m}$ remains narrow and centered on ρ_f.

In the range of fugacities $\exp(\beta\mu_f)$ considered for each isotherm 10 to 25 simulations have been realized. For each matrix configuration 80×10^6 Monte Carlo (MC) trial moves have been performed; averages were taken over 6–10 different matrix configurations in the gas phase and 10–12 configurations in the liquid phase. Near the phase transitions, averages were taken over 20–42 matrix configurations. With 80×10^6 MC trial moves the fluid densities for one matrix configuration could be estimated with a precision of the order of 0.1–0.2 %. The estimate of the error of the densities averaged over the matrix configurations can obviously be biased by using too small a number of these configurations. From error analysis using sub-blocks in calculations with $\sim$40 matrix configurations, we conclude that the error of the fluid densities can reliably be estimated to be 2–3 % if the number of matrix configurations is $\sim$10.

V. RESULTS

A. Comparison with simulations

The computer simulations, carried out for four different matrix densities $\rho_0=0$, 0.05, 0.15, and 0.3 at $\alpha=0.7$,$y=1$,$z\sigma=2.5$, and $r_c=2.5\sigma$, have been compared with ORPA results. MC results for isotherms of the bulk system, $\rho_0=0$, and adsorption isotherms of the system with lowest porosity, $\rho_0=0.3$, are shown in Figs. 6 and 7. In the range of temperatures $T\approx0.7$–0.8 one observes, for $\rho_0=0$, a first order *G-L* transition with critical temperature $T_c\approx0.72$–0.73 and critical density $\rho_c\approx0.35$ and a line of second order demixing transitions terminating at a tricritical point with temperature $T_{tc}\approx0.73$, slightly higher than the critical temperature, and density $\rho_{tc}\approx0.57$. This diagram is of type II. When the matrix density increases, the temperature range within which the equimolar liquid exists decreases and the phase diagram evolves toward a type I diagram. At $\rho_0=0.3$ the phase diagram in the temperature range 0.49–0.52 reveals that (within the accuracy of the simulation results) the tricritical temperature, or possibly the temperature of the critical end point, is close to and slightly below the critical temperature ($\sim$0.51).

Comparison of the phase diagrams with ORPA results is illustrated in Fig. 8. At $\rho_0=0$ excellent agreement is obtained for the *G-L* and *L-DF* transition densities, the fluid concentrations of the demixed phase, and the λ line. This agreement deteriorates, however, with increasing ρ_0. Although in the ORPA the same sequence of types of phase diagram occurs as in the simulations and general trends (lowering of the critical temperature and narrowing of the *G-L* coexistence curve with increasing matrix density) are correctly reproduced, marked differences are observed on a quantitative level. In particular, for $\rho_0\geqslant0.15$, the critical temperature is found to be higher than in the simulations; also the ratio of the critical to tricritical or end point temperature increases with ρ_0, while it remains close to 1 in the

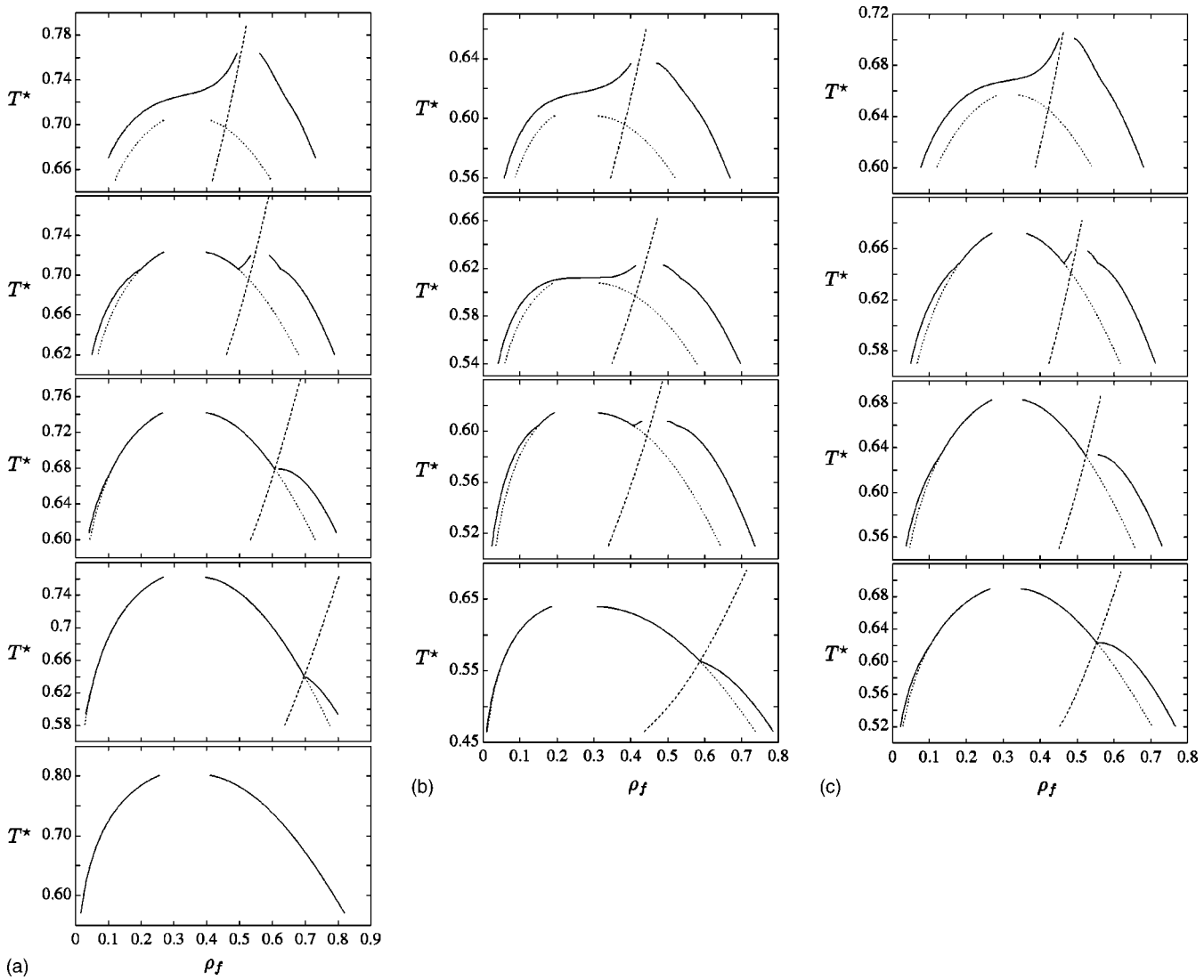

FIG. 10. Variation with α of the phase diagram of the binary fluid mixture in thermal equilibrium with a porous matrix from ORPA. (a) $(\rho_0=0)$: $\alpha=0.65$, 0.70, 0.75, 0.80, and 0.90 (from top to bottom); (b) $(\rho_0=0.1, y=0)$: $\alpha=0.68$, 0.70, 0.72, and 0.80 (from top to bottom); (c) $(\rho_0=0.1, y=1)$: $\alpha=0.65$, 0.70, 0.73, and 0.75 (from top to bottom). Full line, *G*-*L*, *G*-DF, or *L*-DF coexistence curves; dotted line, metastable *G*-*L* transition; dashed line, λ line.

simulations. Furthermore, the critical density shifts to lower values in contrast to the simulations where it remains nearly constant. On the other hand, the concentrations of the demixed phase remain accurate even at a high matrix density as illustrated in Fig. 9 for $\rho_0=0.15$. As noted in the previous section, the determination of the equilibrium densities of the different phases in the simulations is affected by uncertainties of the order of 2–3 % for $\rho_0\neq 0$ and ~1 % for $\rho_0=0$. In view of these error bars the difference between the theory and the simulations at the higher matrix densities is significant. The major source of error is likely to be found in the use of the ORPA, in particular in that of the PY type closure to solve the ROZ equations for the reference hard-sphere system in the framework of the replica theory [24]. Differences of similar size between simulation and ORPA results were observed in the one component case [25].

B. Variation of α

The variation of the phase diagram with α (ratio of the interaction strengths of unlike and like particles) is shown in Fig. 10 for the matrix densities $\rho_0=0$ and 0.1. In the latter case the matrix-fluid interaction was either a pure hard-sphere $(y=0)$ or a hard-sphere + Yukawa interaction $(y=1)$. For the bulk mixture we observe—in qualitative agreement with the mean-field results of Wilding *et al.* [13]—variation of the phase diagram from type III to type II to type I as we increase α from 0.65 to 0.90. At $\alpha=0.9$ no demixing transition could be observed down to a temperature $T=0.55$, below which the ORPA equations could no longer be solved. At this temperature and α value a freezing transition is also possible and the demixing transition no longer exists in the fluid phase. Over the range of α values considered the critical temperature and density do not vary appreciably with

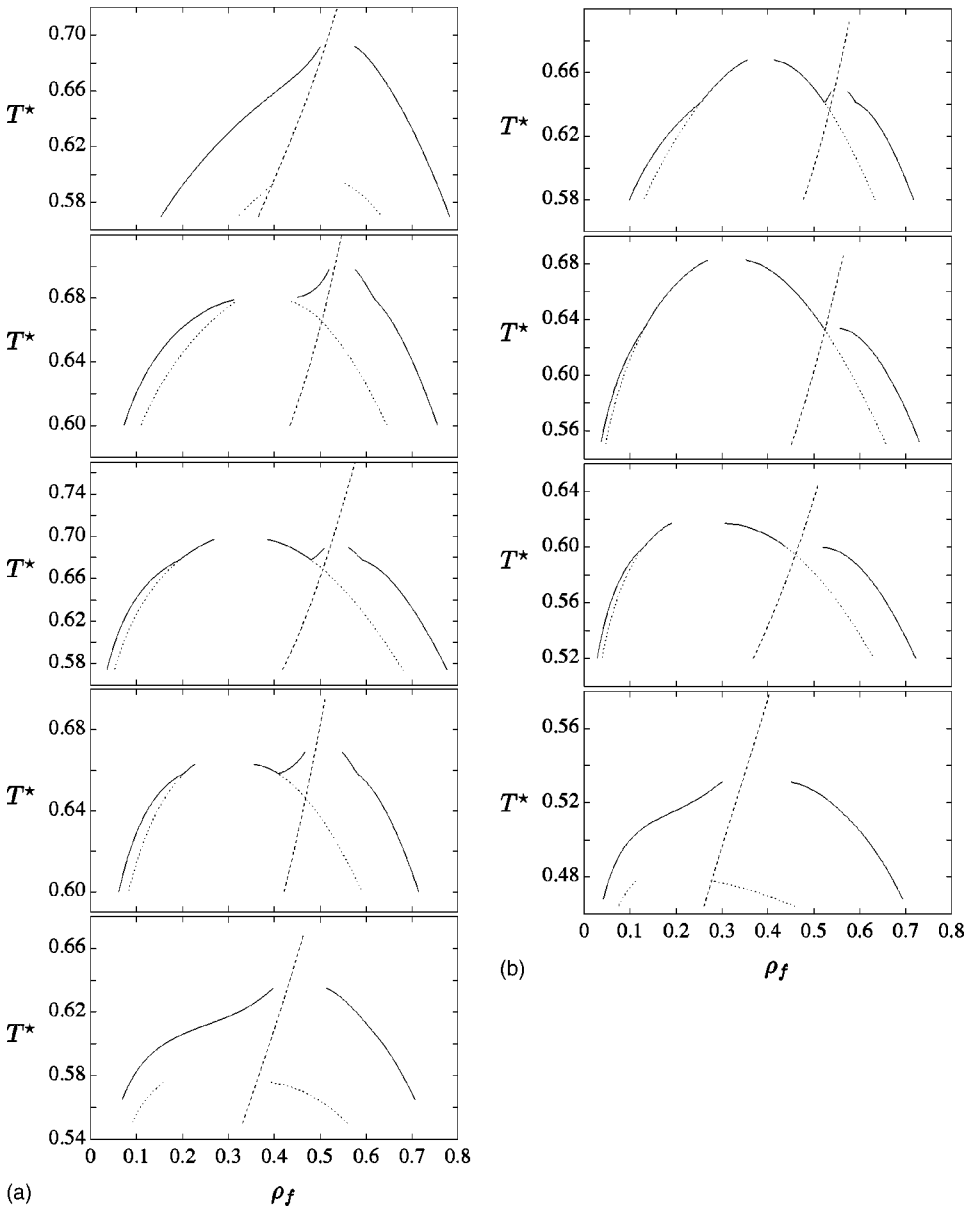

FIG. 11. Variation with y of the phase diagram of the binary fluid mixture in thermal equilibrium with a porous matrix from ORPA. (a) ($\rho_0=0.05,\alpha=0.7$): $y=3.5,2,1,0,-1$ (from top to bottom); (b) ($\rho_0=0.10,\alpha=0.73$): $y=2,1,0,-1$ (from top to bottom). Full line, *G-L*, *G*-DF, or *L*-DF coexistence curves; dotted line, metastable *G-L* transition; dashed line, λ line.

α. An increase of the matrix density from 0 to 0.1 (at $y=1$) does not alter this behavior or the sequence of phase diagrams (from type III to type I) but lowers T_c and T_{tc} by $\sim$10% and shifts the densities of the tricritical and CEP points to slightly lower densities. A change of y from 1 to 0 at fixed matrix density $\rho_0=0.1$ lowers T_c by $\sim$10%, shifts ρ_c from $\sim$0.32 to $\sim$0.26, and delays the appearance of the CEP as one increases α.

C. Variation of *y*

The variation with the parameter y (expressing the ratio between the fluid-fluid and the matrix-fluid interactions) is shown in Fig. 11 for the two cases $\rho_0=0.05,\alpha=0.7$ and $\rho_0=0.1,\alpha=0.73$. A positive value of y represents an attraction between matrix and fluid particles while a negative value represents a repulsion. For the lower matrix density $\rho_0=0.05$, the sequence of phase diagrams is found to be type III→type II→type III when y decreases from positive to negative values. A *G-L* transition appears near $y\sim2$ (a precise location cannot be found due to numerical problems in the critical region as mentioned above) and exists only in a small range of y values extending roughly from 2 to -0.5. The phase diagram is again of type III for the more strongly repulsive matrix-fluid interactions $y=-1$. A qualitatively similar behavior is observed for the larger matrix density $\rho_0=0.1$; here the type II phase behavior occurs at least for $0<y<2$.

The ORPA allows us to determine the metastable *G-L* transitions (hidden below the *G-DF* coexistence curve); these are marked in Fig. 11 by dotted lines. From the figure, it is apparent that, when the matrix is strongly attractive ($y=3.5$), the λ line (extended into the *G-DF* coexistence region) intersects the metastable first order *G-L* coexistence line at a density smaller than the (metastable) critical density $\rho_c^{\mathrm{G\text{-}L}}$, while for the repulsive matrix-fluid interaction ($y=-1$) the intersection is observed for densities larger than

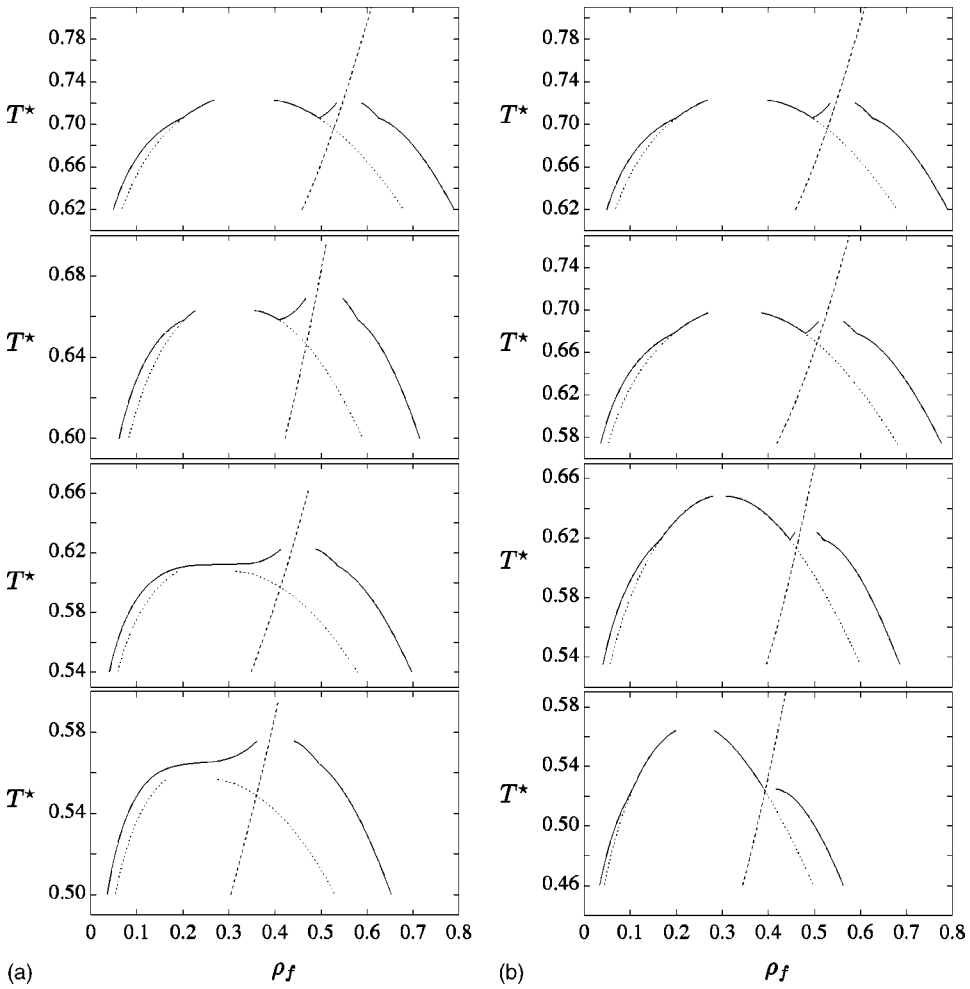

FIG. 12. Variation with matrix density ρ_0 of the phase diagram of the binary fluid mixture in thermal equilibrium with a porous matrix from ORPA. (a) ($y=0,\alpha=0.7$): $\rho_0=0$, 0.05, 0.10, and 0.15 (from top to bottom); (b) ($y=1,\alpha=0.7$): $\rho_0=0$, 0.05, 0.15, and 0.30 (from top to bottom). Full line, *G-L*, *G-DF*, or *L-DF* coexistence curves; dotted line, metastable *G-L* transition; dashed line, λ line.

$\rho_c^{\text{G-L}}$. As pointed out by Wilding *et al.* [13] in their mean-field study of a symmetric binary *bulk* mixture, these differences in the metastable equilibrium may be of relevance for the dynamic properties of the system. Therefore, when, in the case of a repulsive matrix, the fluid is quenched from a high temperature state into the coexistence region slightly below the metastable critical point one can expect ''two stage demixing.'' This means, that the system will first separate into a *G* and a *L* phase; then the equimolar liquid will demix [13]. In contrast, for an attractive matrix ($y=3.5$), the fluid will demix and phase separate simultaneously (''one-stage demixing'' [13]).

D. Variation of ρ_0

The influence of the matrix density on the phase diagram of the mixture is shown in Fig. 12 for two values 0 and 1 of the parameter y and $\alpha=0.7$. As discussed in the comparison of simulation and theoretical results, in both cases, at $\rho_0=0$, we have a type II diagram characterized by a tricritical point where the λ line of the second order demixing transition terminates as well as a triple point where the *G*, the *L*, and the *DF* coexist. As we increase ρ_0, at $y=1$ (attractive tail in the matrix-fluid interaction) the tricritical temperature T_{tc} decreases; at $\rho_0\sim 0.3$ the first order transition between the *L* and the *DF* has vanished, giving rise to a CEP at T_{cep} (type I phase diagram). It can be seen that the existence of a CEP leads to a kink in the *G-L* curve, clearly visible in the ORPA data, a phenomenon that has been discussed in a simulation study of the pure mixture in [26]. The situation is completely different if the matrix-fluid interactions are hard-sphere potentials ($y=0$). We now arrive with increasing ρ_0 at a type III phase diagram; for $\rho_0\sim 0.1$ the *G-L* transition becomes metastable and hidden below the *G-DF* transition (type III phase diagram). As discussed in the previous subsection, the metastable *G-L* transition can lead to a two stage demixing.

E. Variations of z and r_c

The change in phase diagram entailed by variation of the screening length z of the Yukawa potential is shown in Fig. 13 for $\rho_0=0.10$, $\alpha=0.68$, and $y=0$. A change of $z\sigma$ from 2 to 3 mainly lowers the tricritical temperature and the critical temperature of the metastable *G-L* transition, but otherwise leaves the critical density and type of phase diagram (type III) unchanged.

Increasing the range of the Yukawa potential from $r_c=2.5\sigma$ (the value at which most of the ORPA calculations have been performed to allow comparison with the MC simulations) to 8σ raises the critical temperature while preserving the shape of the phase diagram (see Fig. 14). We observe a narrowing of the *G-L* coexistence region.

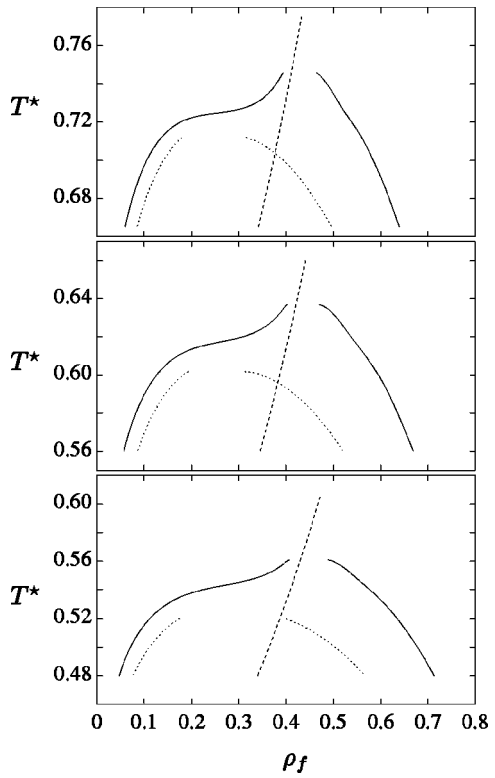

FIG. 13. Variation with screening length z of the phase diagram of the binary fluid mixture in thermal equilibrium with a porous matrix from ORPA. Parameters: $y=0$, $\alpha=0.68$, and $\rho_0=0.10$. $z\sigma=2$, 2.5, and 3 (from top to bottom). Full line, *G-L*, *G-DF*, or *L-DF* coexistence curves; dotted line, metastable *G-L* transition; dashed line, λ line.

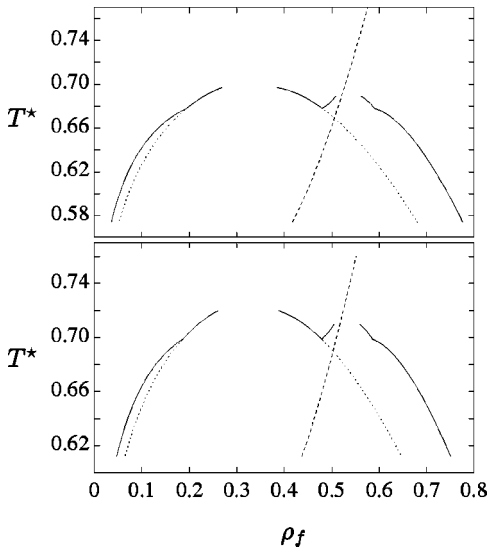

FIG. 14. Variation with cutoff radius r_c of the phase diagram of the binary fluid mixture in thermal equilibrium with a porous matrix from ORPA. Top curve, $r_c=2.5\sigma$; bottom curve, $r_c=8\sigma$. The other parameters are $y=1$, $\alpha=0.7$, and $\rho_0=0.05$. Full line, *G-L*, *G-DF*, or *L-DF* coexistence curves; dotted line, metastable *G-L* transition; dashed line, λ line.

VI. CONCLUSIONS

Results obtained within the framework of the ROZ integral equation theory in combination with the ORPA closure have provided detailed information on the influence of matrix density and parameters defining the interactions between the particles of the (symmetric) binary mixture and between the mixture and the matrix particles.

Mean-field theory predicts for a binary symmetric bulk mixture (of the type considered here) the existence of three generic phase diagrams. These phase diagrams are also obtained in the present study by the ROZ theory and by simulation for both the bulk and adsorbed mixtures. A major achievement of this work is to supply a nonambiguous correspondence between the interactions in the partly quenched system (mixture plus porous matrix) and the type of phase diagram to which they give rise. In the bulk binary mixture the change in phase diagram is triggered by only one parameter (the parameter α); this is also the case in other bulk systems, such as for instance the Heisenberg or Stockmayer fluid where the change in the type of phase diagram is triggered by the ratio of the strengths of the isotropic and anisotropic interactions [27,28]. In the present system the situation is more complex, bringing into play a combination of several parameters α, y (the ratio of fluid-fluid and matrix-fluid interactions), and the porosity (via ρ_0). Small changes in each of these parameters have been shown to lead to qualitative changes of the phase diagrams. In particular, for a given fluid and matrix, it is apparent that the phase diagram can be changed drastically by varying the porosity of the medium, which is the parameter most readily controllable in experiment.

In the simulations, care has been taken to average over a sufficiently large number of matrix configurations to reduce the systematic statistical error to the level of a few percent. Finite size effects have not been taken into account so far. Outside the critical region, previous simulations performed for a one component fluid in a hard-sphere matrix [25] for different system volumes do not reveal notable quantitative size effects on the system properties. In the critical region, in the absence of a firmly established scheme for analysis of finite size effects in a disordered medium, the latter are difficult to estimate. They can possibly shift the critical or tricritical point by a small amount, although the effect is expected to be too small to preclude a quantitative comparison between theory and simulations.

Comparison between simulations and theory has disclosed the necessity for improving ORPA theory in the domain of matrix densities $\rho_0>0.1$. Effort in this direction is in progress. We also plan to extend theory and simulations to systems comprising long range Coulomb and dipolar interactions such as electrolyte solutions.

ACKNOWLEDGMENTS

This work was supported by the Österreichische Forschungsfond under Projects No. P13062-TPH, No. P14371-TPH, and No. W004, the Wiener Handelskammer, and a grant through the Programme d'Actions Intégrées AMADEUS. E.P. and G.K. acknowledge the warm hospitality at

the Laboratoire de Physique Théorique (Université de Paris-Sud, Orsay), where part of this work was done. We also would like to thank Dr. E. Lomba (CSIC, Madrid) for providing a copy of his integral equation code. Computing time on the Cray C-98 was granted by the Institut de Dévelopement et de Ressources en Informatique (IDRIS). Computational aid by Dieter Gottwald (TU Wien) is gratefully acknowledged.

[1] M.-L. Rosinberg, in *New Approaches to Problems in Liquid State Theory*, Vol. 529 of *NATO Science Series*, edited by C. Caccamo, J.-P. Hansen, and G. Stell (Kluwer, Dordrecht, 1999).

[2] See, e.g., B. J. Frisken, F. Ferri, and D. S. Cannell, Phys. Rev. E **51**, 5922 (1995), and references therein; Z. Zhuang, A. G. Casielles, and D. S. Cannell, Phys. Rev. Lett. **77**, 2969 (1996); J. V. Maher, W. I. Goldburg, D. W. Pohl, and M. Lanz, *ibid.* **53**, 60 (1984).

[3] See, e.g., M. C. Goh, W. I. Goldburg, and C. M. Knobler, Phys. Rev. Lett. **58**, 1008 (1987); S. B. Dierker and P. Wiltzius, *ibid.* **58**, 1865 (1987); P. Wiltzius, S. B. Dierker, and B. S. Dennis, *ibid.* **62**, 804 (1989); S. B. Dierker and P. Wiltzius, *ibid.* **66**, 1185 (1991); F. Aliev, W. I. Goldburg, and X-L. Wu, Phys. Rev. E **47**, 3834 (1993); M. Y. Lin, S. K. Sinha, J. M. Drake, X.-L. Wu, P. Thiyagarajan, and H. B. Stanley, Phys. Rev. Lett. **72**, 2207 (1994); S. Lacelle, L. Tremblay, Y. Bussière, F. Cau, and C. G. Fry, *ibid.* **74**, 5228 (1995); D. J. Tulimieri, J. Yoon, and M. H. W. Chan, *ibid.* **82**, 121 (1999); F. Formisano and J. Teixeira, Eur. Phys. J. E **1**, 1 (2000).

[4] W. G. Madden and E. G. Glandt, J. Stat. Phys. **51**, 537 (1988); W. G. Madden, J. Chem. Phys. **96**, 5422 (1992).

[5] J. A. Given, Phys. Rev. A **45**, 816 (1992).

[6] J. A. Given, J. Chem. Phys. **96**, 2287 (1992).

[7] J. A. Given and G. Stell, Physica A **209**, 495 (1994).

[8] S. F. Edwards and P. W. Anderson, J. Phys. F: Met. Phys. **5**, 965 (1975); S. F. Edwards and C. Jones, J. Phys. A **9**, 1595 (1976).

[9] J.-P. Hansen and I. R. McDonald, *Theory of Simple Liquids*, 2nd ed. (Academic Press, New York, 1986).

[10] M.-L. Rosinberg, G. Tarjus, and G. Stell, J. Chem. Phys. **100**, 5172 (1994).

[11] E. Kierlik, M.-L. Rosinberg, G. Tarjus, and P. Monson, J. Chem. Phys. **103**, 4256 (1995).

[12] E. Paschinger and G. Kahl, Phys. Rev. E **61**, 5330 (2000).

[13] N. B. Wilding, F. Schmid, and P. Nielaba, Phys. Rev. E **58**, 2201 (1998).

[14] M. P. Allen and D. J. Tildesley, *Computer Simulations of Liquids* (Clarendon, Oxford, 1990).

[15] H.C. Andersen and D. Chandler, J. Chem. Phys. **57**, 1918 (1972); H.C. Andersen, D. Chandler, and J.D. Weeks, *ibid.* **56**, 3812 (1972).

[16] E. Kierlik, M.L. Rosinberg, G. Tarjus, and P.A. Monson, J. Chem. Phys. **106**, 264 (1997); **110**, 689 (1999).

[17] D.M. Ford and E.D. Glandt, J. Chem. Phys. **100**, 2391 (1994).

[18] A. Parola and L. Reatto, Adv. Phys. **44**, 211 (1995).

[19] S. Labik, A. Malijevsky, and P. Vonka, Mol. Phys. **56**, 709 (1985).

[20] E. Lomba, J.A. Given, G. Stell, J.-J. Weis, and D. Levesque, Phys. Rev. E **48**, 233 (1993).

[21] E. Paschinger, Diploma thesis, Technische Universität Wien 1999.

[22] A.M. Ferrenberg and R.H. Swendsen, Phys. Rev. Lett. **61**, 2635 (1988); **63**, 1195 (1989).

[23] J.J. Potoff and A.Z. Panagiotopoulos, J. Chem. Phys. **109**, 10914 (1998).

[24] A. Meroni, D. Levesque, and J.-J. Weis, J. Chem. Phys. **105**, 1101 (1996).

[25] M. Álvarez, D. Levesque, and J.-J. Weis, Phys. Rev. E **60**, 5495 (1999).

[26] N.B. Wilding, Phys. Rev. Lett. **78**, 1488 (1997); Phys. Rev. E **55**, 6624 (1997).

[27] J.-J. Weis, M.J.P. Nijmeijer, J.M. Tavares, and M.M. Telo da Gama, Phys. Rev. E **55**, 436 (1997); J.M. Tavares, M.M. Telo da Gama, P.I.C. Teixeira, J.-J. Weis, and M.J.P. Nijmeijer, Phys. Rev. E **52**, 1915 (1995).

[28] B. Groh and S. Dietrich, Phys. Rev. Lett. **72**, 2422 (1994); in *New Approaches to Problems in Liquid State Theory* (Ref. [1]).